KECK Geology Consortium
Learning Science Through Research
Published by the Keck Geology Consortium
Short Contributions
Keck Geology Consortium
Volume 35
May 2023
doi: 10.18277/AKRSG.2023.35.04

NORMAL FAULT-TIP DAMAGE ZONE STRUCTURES AND GEOMETRIES FROM THE SEVIER FAULT, UTAH

MICHELLE NISHIMOTO, Wellesley College
Project Advisor: Katrin Monecke

INTRODUCTION

Fractures within rocks form due to differential stresses that exceed rock strength. The magnitude and orientation of the local stress field depends on tectonic setting and influences the extent and direction of fracture initiation and propagation. Understanding fracture network characteristics and geometries is fundamental to answer various geological research questions. Studies by Ampuero and Mao (2017) and others have shown the importance of understanding the geometry and intensity of fracturing at and adjacent to faults when evaluating earthquake hazards. In addition, fracturing and the resultant porosity and permeability of a rock affect fluid flow and the potential for geothermal energy transfer (e.g., Siler et al., 2018). Furthermore, fracture pattern analysis may reveal potential asymmetry of fracture intensity across a fault (e.g., Berg and Skar, 2005) and how normal faults grow over time (e.g., Nicol et al., 2016).

For this study, I analyzed the fracture pattern of the isolated normal fault tip zone of the Spencer Bench segment from the Sevier fault using traditional geological field methods as well as a relatively new approach based on analysis of virtual outcrop models built from drone imagery. Both field measurements and virtual outcrop data are used to map the scale and type of fracturing in the fault core and across the adjacent footwall and hanging wall of the fault segment. I explore how fracture intensity varies within the rock volume adjacent to the tip of a normal fault, the difference in fracture network characteristics between the hanging wall and footwall, and the relationship between fracture patterns and lithology.

BACKGROUND

Fault Propagation and Fault Damage Zones

Differences in bed contacts, thickness of beds, and material properties influence the formation and propagation of fractures in sedimentary rocks (e.g., Cooke et al., 2000). Fractures, including faults, initiate and propagate when stress surrounding the rock exceeds rock strength. The extent of the fracture depends on the magnitude and orientation of the local stress field. When normal faults propagate laterally and accommodate displacement across the fault, they often produce a highly deformed fault core and a broader volume of rock deformation known as a damage zone. Based on their location along the fault, damage zones are classified as tip-, wall-, or linking-damage zones (see Fig. 3 in Surpless, this volume). Fault-tip and wall damage zones develop in response to fault propagation and displacement, caused by the local amplification of stresses parallel to the fault plane and in the fault tip regions (e.g., Kim et al., 2004). Damage zones of normal faults can further be divided into inner and outer damage zones developing adjacent to the fault (Fig. 1). As the distance from the fault core increases, the intensity of fracturing decreases to an undamaged rock volume.

Fault Damage Zone Asymmetry

Across a fault, deformation or strain is often distributed asymmetrically, resulting in differences in damage zone characteristics in the hanging wall relative to the footwall (Fig. 1). Along normal faults, the hanging-wall damage zone tends to be wider than the footwall damage zone (Liao et al., 2020). In a study looking at the spatial arrangement of fractures

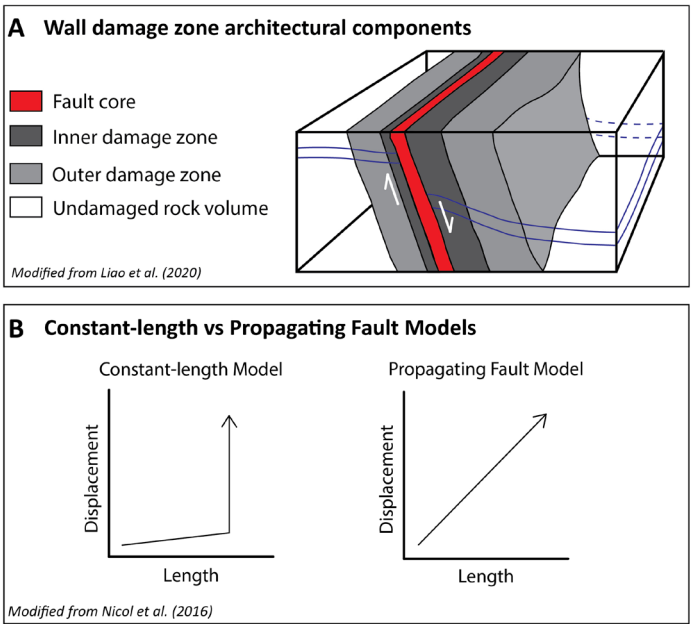

Figure 1. A) Conceptual model for an asymmetrical normal fault wall damage zone and its architectural components. Red indicates the fault core, dark gray is for the inner damage zone, gray is for the outer damage zone, and white marks the undamaged rock. The white arrows and blue lines indicate displacement along the fault and displaced hypothetical rock units. B) Evolution of displacement and length according to the constant-length model (left) and propagating fault model (right). Figure A modified from Liao et al., (2020). Figure B adapted from Nicol et al., (2016).

in the damage zone at a segment of the Moab fault in southeastern Utah, Berg and Skar (2005) found that the hanging-wall damage zone was more than three times wider than the footwall damage zone and suggest that the stress pattern that occurs during fault propagation causes an asymmetric distribution of strain.

Constant-length vs Propagating Fault Models

There are two schools of thought on how a normal fault's displacement (D) and map-view trace length (L) grow over time (Fig. 1): the propagating fault model, also known as the increasing length model or isolated fault model, and the constant-length model, also known as the coherent fault model (Fig. 1) (e.g., Cartwright et al., 1995). The propagating fault model suggests that a fault's D/L ratio stays relatively constant over successive fault movements whereas the constant-length model suggests that there is an initial phase of rapid fault propagation along strike followed by a more prolonged period of displacement accumulation on faults with near-constant lengths (Nicol et al., 2016).

Earlier studies, focused upon map-view geologic data, supported the propagating fault model (e.g., Cartwright et al., 1995). However, more recent studies based on seismic survey data (Walsh et al., 2003), comparisons of the thickness versus displacement of fault geometric components (fault rock, fault zone, breached relay zone, and intact relay zone) of a normal fault (Childs et al., 2009), and a study on a system of faults at outcrop-scale (Nicol et al., 2016) better support the constant-length model. In their study of a fault zone in central Texas, Ferrill et al. (2011) argue that a constant-length model is more consistent with their data and suggest that both fault length and damage zone width are established early and likely remain relatively constant as displacement accumulates.

Sevier Fault Zone

Along the Hurricane and Paunsaugunt normal faults, the Sevier-Toroweap normal fault accommodates strain across the transition zone between the Colorado Plateau to the East and the Basin and Range province to the West (e.g., Davis, 1999; Schiefelbein, 2002; Surpless and McKeighan, 2022) (see Fig. 1 in Surpless, this volume). The Sevier fault is a segmented fault that extends ~350 km through Utah and Arizona with a strike of ~N30°E and steep 70-85°W dip (Davis, 1999; Schiefelbein, 2002). In this study, I focus on an isolated normal fault tip near the southern end of a complexly faulted zone of the Sevier normal fault that is well exposed at the Elkheart Cliffs and the southern end of the Red Hollow Canyon by Orderville, Utah (Fig. 2 in Surpless, this volume).

METHODS

Field Methods

We conducted fieldwork near Orderville, Utah, where there is good exposure of the Spencer Bench Fault segment. At locations of interest, we collected scanline data to document the primary orientation and intensity of fracturing, with the position measured perpendicular to the dominant fracture strike. We used a Geo Transit Brunton to measure the azimuth and dip of each fracture along the scanline and constructed stereonets using Stereonet 11 by Allmendinger (2022).

Capturing Imagery with Unmanned-Aerial-Vehicle (UAV) Flights

In locations inaccessible by foot, we planned and executed a series of unmanned-aerial-vehicle (UAV) flights using a Phantom 4 Professional UAV. The 4K camera attached to the drone recorded video imagery of canyon walls and cliff faces across the fault network. We documented the spatial extent of each drone flight on Google Earth Professional and described the content of each video in a field book.

Building virtual outcrop models (VOMs) using Structure-from-Motion (SfM) software

We used videos taken by the UAV flights to build virtual outcrop models (VOMs) using Agisoft Metashape, structure-from-motion (SfM) software designed to build 3D outcrop models based on overlapping aerial images (Metashape, 2023) (Fig. 2). We created 2D orthomosaics from the georeferenced VOMs, which we annotated in Metashape. Where best exposed, we documented displacement across the fault core. We set up virtual scanlines drawn perpendicular to fractures, measuring the position of fractures along each scanline and conducted statistical analysis on the collected scanline data. Values derived include the average spacing between fractures (m), the fracture spacing standard deviation (m), position-based fracture intensity (FI) (m^{-1}), scanline average FI (m^{-1}), and coefficient of variation (CV =σ/μ).

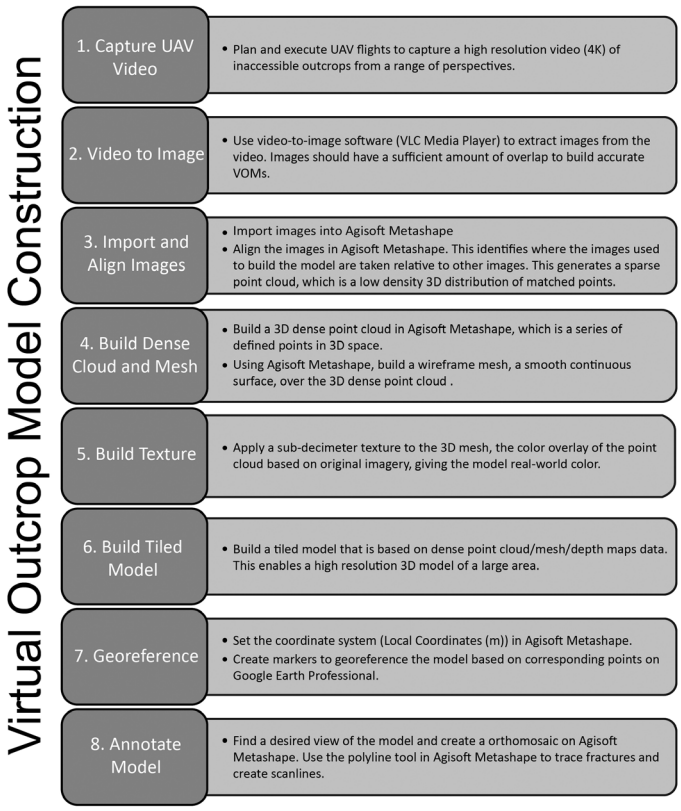

Figure 2. Steps for VOM model construction and analysis. Workflow to construct a spatially accurate 3D outcrop model using Agisoft Metashape. Figure modified from Surpless and McKeighan, 2022.

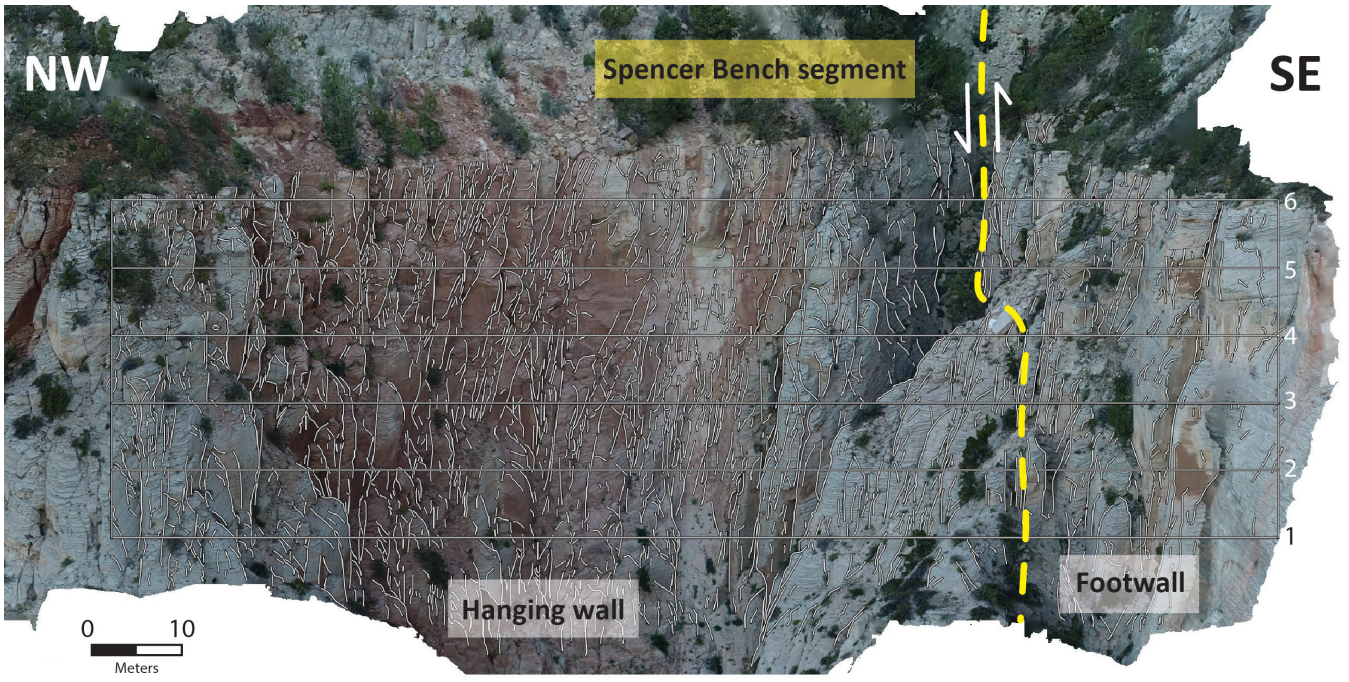

Figure 3. Orthomosaic of Model 3 where the Spencer Bench segment can be seen passing through the model. Yellow dashed lines show the suggested locations where the Spencer Bench segment passes through. White lines trace the fractures observed. White horizontal lines indicate the location of the scanlines.

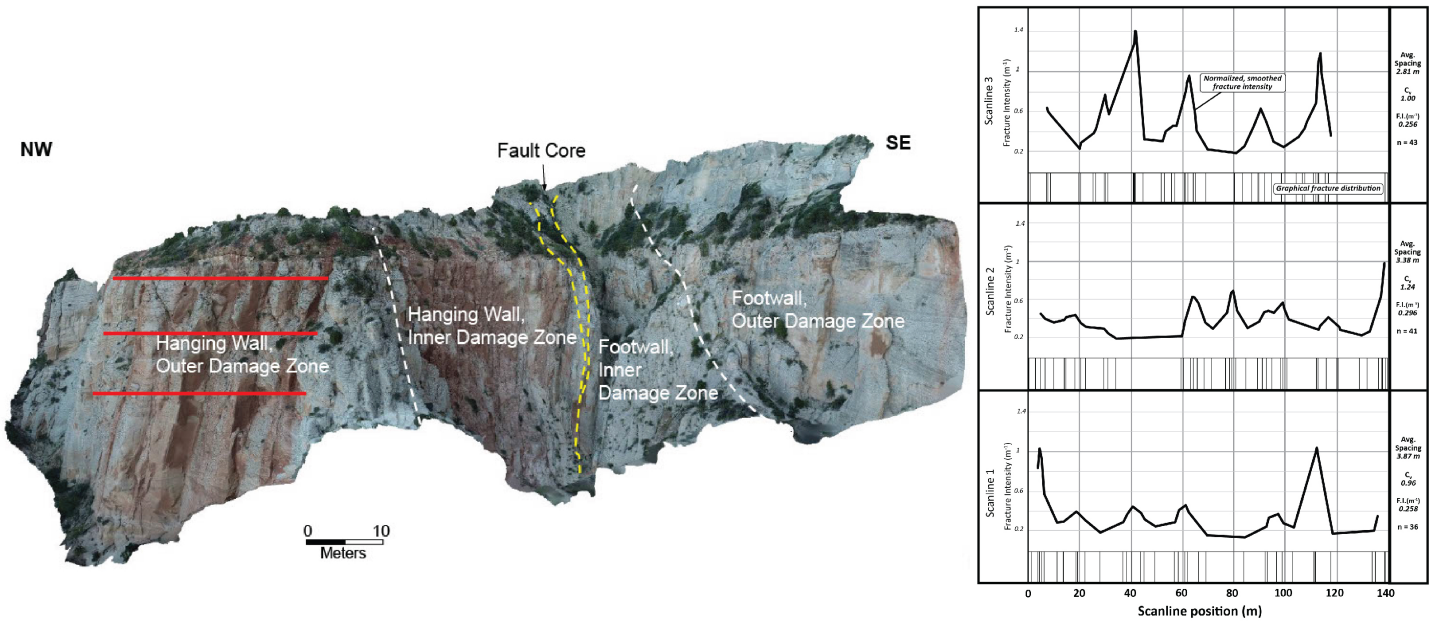

Figure 4. Fault damage zone asymmetry of Model 3 and FI along scanlines. Model 3 shows the Navajo Sandstone across the Spencer Bench segment (yellow). Red lines indicate where scanline data were collected.

RESULTS

Field-Based Scanline Analysis

We collected scanline data at 11 locations within the fault zone of the Mt. Carmel and Spencer Bench segments, focusing on the well-exposed Navajo Sandstone. We measured fractures greater than 4 meters along field scanlines that intersected the strike of the fractures. Overall, most fractures strike NE to NNE and dip moderately to steeply NW, subparallel to the fault segments. The average FI ranged between 0.19 m^{-1} and 6.31 m^{-1}.

Fault Damage Zone Asymmetry

Observations from Model 3, at Elkheart Cliffs with the Spencer Bench segment located on the SE side of the model, support the analysis performed by Liao et al., (2020) and Berg and Skar (2005), who suggested that wall damage zones display greater widths of both inner and outer damage in the hanging wall relative to the footwall (Figs. 3 and 4). This asymmetry may result from preferential fracture rupture propagation caused by footwall-hanging wall differences in local stress fields around normal fault planes (e.g., Ampuero and Mao, 2017). Our finding is significant given we documented damage zone widths based on outcrop exposures, unlike Liao et al., (2020), where seismic data were used to identify the asymmetry.

Constant-length vs Propagating Fault Models

A comparison of the widths of the footwall damage zone of the Mt. Carmel and Spencer Bench segments at the same latitude shows near-identical dimensions (Fig. 5). However, the displacement across the Mt. Carmel segment is approximately 800 meters (McKeighan et al., 2019), while the displacement across the Spencer Bench segment is only about 2 meters. This suggests that the two faults at this latitude are at different stages of fault propagation and that

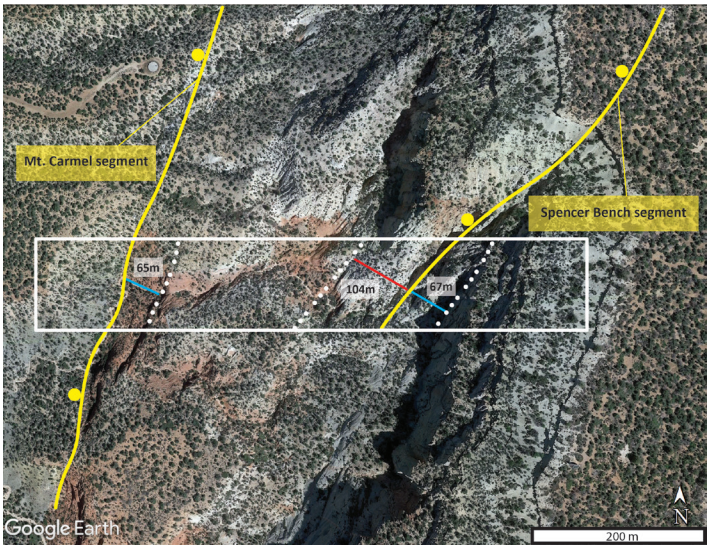

Figure 5. Comparison of the width of the footwall damage zones of the Mt. Carmel and Spencer Bench segments (blue) at the same latitude. Width measurements are taken perpendicular to the fracture orientation from Google Earth Professional.

the footwall damage zone width is established very early in fault propagation. New damage will likely be localized in the already established damage zone (e.g., Ferrill et al., 2011). In addition, McKeighan et al. (2019) identified displacement of 30 meters across the Spencer Bench segment approximately 2.5 kilometers North of where we measured a displacement of only 2 meters in Model 2. This yields a low lateral displacement gradient of 0.0112. Together, this suggests relatively rapid lateral propagation of the Spencer Bench segment with little accumulated displacement. These data strongly support the constant-length model.

ACKNOWLEDGMENTS

This material is based upon work supported by the Keck Geology Consortium and the National Science Foundation under Grant No. 2050697. It was also supported by NSF Award 2042114 to PI Surpless. I would like to extend my deepest gratitude to Dr. Benjamin Surpless and Dr. Katrin Monecke for their continuous support throughout this project.

REFERENCES

Allmendinger, R., 2022. Stereonet 11: accessed January, 2023, https://www.rickallmendinger.net/stereonet/

Ampuero, J. P., and X. Mao, 2017, Upper limit on damage zone thickness controlled by seismogenic depth, in M. Y. Thomas, T. M. Mitchell, and H. S. Bhat, eds., Fault zone dynamic processes: Evolution of fault properties during seismic rupture: American Geophysical Union, doi: 10.1002/9781119156895.ch13.

Berg, S., and T. Skar, 2005, Controls on damage zone asymmetry of a normal fault zone: Outcrop analyses of a segment of the Moab fault, SE Utah: Journal of Structural Geology, 27, 1803–1822, doi: 10.1016/j.jsg.2005.04.012.

Cartwright, J.A., Trudgill, B.D., and Mansfield, C.S., 1995, Fault growth by segment linkage: an explanation for scatter in maximum displacement and trace length data from the Canyonlands Grabens of SE Utah: Journal of Structural Geology, v. 17, no. 9, p. 1319-1326.

Childs, C., Manzocchi, T., Walsh, J.J., Bonson, C.G., Nicol, A., and Schopfer, M.P.J., 2009: A geometric model of fault zone and fault rock thickness variations: Journal of Structural Geology, v. 31, p. 117-127.

Cooke, M., Mollema, P., Pollard, D., and Aydin, A., 2000, Interlayer slip and joint localization in the East Kaibab Monocline, Utah: field evidence and result from numerical modeling, In Cosgrove, J., and Ameen, M., eds.: Forced Folds and Fractures, Geological Society, London, v. 169, p. 23-49.

Davis, G., 1999, Structural geology of the Colorado Plateau region of southern Utah, with special emphasis on deformation bands: Geological Society of America Special Paper 342, p. 157.

Ferrill, D.A., Morris, A.P., McGinnis, R.N., Smart, K.J., and Ward, W.C., 2011, Fault zone deformation and displacement partitioning in mechanically layered carbonates: the Hidden Valley fault, central Texas: The American Association of Petroleum Geologists, v. 95, no. 8, p. 1383-1397.

Kim, K.S., Peacock, D., and Sanderson, D., 2004, Fault damage zones: Journal of Structural Geology, v. 26, p. 503– 517.

Liao, Z., Hu, L., Huang, X., Carpenter, B., Marfurt, K., Vasileva, S., Zhou, Y., 2022, Characterizing damage zones of normal faults using seismic variance in the Wangxuzhuang oilfield, China: Interpretation, v. 8, doi: 10.1190/INT-2020-0004.1.

Metashape, Agisoft, 2023. Agisoft Metashape User Manual (pdf): accessed March, 2023.https://www.agisoft.com/pdf/metashape-pro_2_0_en.pdf. version 2.0.

McKeighan, C., and Surpless, B., 2019, Analyzing Deformation within a Normal Fault Transfer Zone Using SfM 3D Modeling: Keck Geology Consortium, Volume of Short Contributions, v. 32, 7 p.

Nicol, A., Childs, C., Walsh, Manzocchi, T., and Schopfer, M.P.J., J.J., 2016, Interactions and growth of faults in an outcrop-scale system: Geological Society of London, v. 439, p. 23-39, doi: 10.1144/SP439.9

Schiefelbein, I.M., 2002, Fault segmentation, fault linkage, and hazards along the Sevier fault,southwestern Utah [M.S. thesis]: Las Vegas, University of Nevada at Las Vegas, 132 p.

Siler, D.L., Hinz, N.H., Faulds, J.E., Tobin, B., Blake, K., Tiedeman, A., Sabin, A., Lazaro, M., Blankenship, D., Kennedy, M., Rhodes, G., Akerley, J., Hickman, S., Glen, J., Williams, C., Robertson-Tait, A., Pettitt, W., 2018, An Update on the Geologic Model of the Fallon FORGE site. Geothermal Research Council Transactions, v. 41, p. 11-21.

Surpless, B., 2023, Structural Evolution of the segmented Sevier fault, southern Utah: Keck Geology Consortium, Volume of Short Contributions, v. 36, 7 p.

Surpless, B., and McKeighan, C., 2022, The role of dynamic fracture branching in the evolution of fracture networks: an outcrop study of the Jurassic Navajo Sandstone, southern Utah: Journal of Structural Geology, v. 161. doi: 10.1016/j.jsg.2022.104664.

Walsh, J.J., Bailey, W.R., Childs, C., Nicol, A., and Bonson, C.G., 2003: Formation of segmented normal faults: a 3-D perspective: Journal of Structural Geology, v. 25, p. 1251-1262.